A NUMERICAL SIMULATION INVESTIGATION OF THE HYDRODYNAMIC MOTIONS OF A SHIP ADVANCING IN WAVES

(DOI No: 10.3940/rina.ijme.2014.a4.309)

D C Lo, D T Su, and J T Lin, National Kaohsiung Marine University, Taiwan

SUMMARY

This study establishes a relationship diagram of the ship-wave interaction under a ship advancing in waves. A finite difference method based on volume of fluid (VOF) principles was used to simulate the hydrodynamic motions of a ship advancing in waves. A ship model was constructed using a computer aided design (CAD) tool. The computational fluid dynamic (CFD) technique was used to calculate the hydrodynamic motions effect of a ship sailing in waves at varying angles of incidence. This study investigates a number of significant related parameters, such as the speed of the ship model, the various wave incidence angles, the wave height, and the navigation time. A chart is also used to show the flow field, and changes in the six degrees of freedom motion and continually compare changes in the drag force.

1. INTRODUCTION

Numerical simulation research has become an important development target in recent years. Although including computational fluid dynamics (CFD) in ship drag force calculations is fairly commonplace now, CFD studies concerning ship maneuvering performance are still in the exploratory stage (Hooyer, 1994)[1]. With rapid developments in the IT industry, increases in the computational speed of personal computers, maturing mesh generation techniques, and improved numerical algorithms, CFD has now achieved substantial precision and reliability in numerical fluid simulation analyses. Simulations and experiments of the interaction between ships and fluid no longer require large-scale ship hydrodynamics laboratories or professional models.

Advancements in ship technology and ship enlargements trend have resulted in substantial disparity between data and theory on the operation of ships and the actual operation of the current in-service fleets. This study applies CFD analysis technique to simulate ship movements that can provide a reference for ship navigators at sea. Lo et al. (2009)[2] used a commercial code to study the bank effects, and by Lo(2012)[3] also investigated on overtaking and head-on encounters. We further investigated ships encountering waves when advancing with a fixed vessel speed. We investigated the representations of the six degrees of freedom, the ship movements, the variations in drag forces and flow field. This study can provide a reference for ship pilots regarding dynamic maneuvers and to maritime researchers and pilot training courses for teaching and training purposes.

During navigation, ships affected by winds and waves exhibit three types of linear movement: heaving, surging, and swaying. Three additional rotational movements along the three axes are rolling, pitching, and yawing. Among these, heaving, rolling, and pitching are affected by restoring forces and restoring torques; thus, they are oscillatory motions. Surging, swaying, and yawing, however, are not affected by restoring forces or restoring torques; thus, they are non-oscillatory motions. The coupling motion of ships in waves is actually an extremely complex issue. To simplify the complexity of ships in regular waves, elastic deformations of rigid hulls are frequently disregarded. Regular waves are defined as deep water waves with small amplitudes, without the effects of shallow water and nonlinearity. The dynamic response of ships in regular waves is considered small amplitude motions. Lewis and Numerate (1960)[4] examined transverse and oblique waves using ship models in regular waves and irregular waves. Their measurements found that the amount of rolling in regular and irregular waves is extremely consistent. Ochi et al. (1964)[5] also proved the effectiveness of applying the superposition principle in rolling movements and proposed that the response amplitude operator (RAO) for rolling response wave amplitude when applying the superposition principle should be first obtained from smaller regular wave experiments to conform to linear rolling motion conditions.

Among the theoretical research methods for seakeeping performance, strip theory (Korvin-Kroukovsky, 1961)[6] overcame the disadvantage of other theories being unable to describe ships with geometric shapes and assumes that the fluid flow at each of the strips is two-dimensional. Additionally, strip theory ignores effect of the fluid in the bow-stern direction, simplifying a three-dimensional problem into two dimensions for consideration. The calculated dynamic response of ships using strip theory remains fairly consistent with ship model test results. However, a new strip theory was proposed in 1969 by Tasai and Takaki (1969)[7] and Salvensen et al. (1970)[8]. They proposed methods to calculate various types of motions and loads for ships in oblique waves. The primary difference is the turbulence calculation methods and whether the bottom effect exists. This further improves the prediction reliability of ship motions in waves.

Wilson et al. (2007)[9] used CFD numerical software to simulate the effects of ship models with various shapes of bulbous bows encountering waves. Compana et al. (2006)[10] used CFD numerical software to simulate hull shape design optimization for ships advancing in waves. Eca and Hoekstra (2009)[11] used resistance coefficients on ship stern flow calculations to predict the accuracy of the results from the numerical models. Toxopeus (2009)[12] proposed using viscous flow calculations to derive mathematical maneuvering models for bare ship hulls. Evaluating the maneuvering behavior of designs using this method requires highly reliable simulation models. Delefortrie and Vantorre (2009)[13] used a fluidization parameter to predict the forces acting on container carriers in muddy navigation areas and evaluated the navigation safety of ships. Guo et al. (2012)[14] presented the prediction of added resistance and ship motion of KVLCC2 in head waves. Ship pitch and heave motion in regular head waves can be calculated accurately by the proposed model. These studies show that the CFD technique is already widely applied in engineering design and fluidic interaction analysis. This study uses a Flow-3D package based on the finite difference method to analyze and discuss the nonlinear interaction between periodic waves and advancing ships. The results of the flow field numerical data and the motion modes of ships in navigation can be used as a reference for pilots during actual operations, increasing vessel navigation.

2. NUMERICAL METHODS

The physical phenomena investigated in this study belong to the field of fluid dynamics. Additionally, the mathematical models presented in this study are solved using the Naviers-Stokes equations. Analytical methods that are currently employed remain unable to fully resolve these partial differential equations. Thus, this study uses a finite difference method to model flow field changes and determine the relevant flow field variables.

2.1 NAVIER-STOKES EQUATIONS

In classical dynamics, the laws of physics that are followed by the matter systems are “conservation of mass” and “conservation of momentum.” For incompressible three dimension viscous fluids, the non-dimensional continuity equation (1) and momentum equation (2) in the orthogonal coordinate system are expressed as follows:

$$\nabla \cdot \mathbf{u} = \frac{\mathrm{RSOR}}{\rho} \tag{1}$$

$$\frac{\partial \mathbf{u}}{\partial t} + (\mathbf{u} \cdot \nabla)\mathbf{u} = -\frac{1}{\rho}\nabla p + \mathbf{G} - \frac{1}{\rho}\Delta\boldsymbol{\tau} - K\mathbf{u} - \frac{\mathrm{RSOR}}{\rho}\mathbf{u} - \mathbf{f} \tag{2}$$

The mass continuity equation and momentum equation in the x, y, and z directions are expressed as above, $\mathbf{u} = (u, v, w)$ represents the instantaneous velocity components in the horizontal and vertical directions, x, y, and z represent the respective coordinates in the horizontal and vertical directions. RSOR , on the right side of Equation (1) is a mass source. P denotes the instantaneous pressure, while ρ refers to the density, and G is the gravity and non-inertial body acceleration. $\boldsymbol{\tau}$ denotes the viscous stress tensor, Ku is the drag components (porous baffles, obstacles, mushy zone), RSOR/ρ is the accelerations caused by mass injection at zero velocity, f denotes other forces (surface tension, electric forces, mass/momentum sources, particles). Note that in performing the simulations, all the unknown variables (u,v,w,p) are solved through the discretization of Eqs. (1, 2).

2.2 VOLUME OF FLUID (VOF) METHOD

Processing free surface variations using numerical methods is extremely difficult. The free surface is not fixed, moving over time. Through fixed mesh grids, the VOF method provides a method to monitor and process the fluid interface accurately. In other words, the VOF method is a numerical method for processing the free surface or interface between two fluid bodies.

The VOF method was jointly proposed by Hirt and Nichols (1981)[15] and defines an additional fluid ratio function $F(x, y, z, t)$ in mesh grid calculations. F is located at the grid center, in the same place as the pressure variable, and its value is between 0 and 1. F=1 means that the fluid body is filled completely, and F=0 means no fluid exists. An F value between 0 and 1 indicates partial filling; the partially filled element is the fluid interface. The control equation for the F function value is shown below.

$$\frac{\partial F}{\partial t} + \frac{1}{V_f}\nabla \cdot (FVA_f) = 0 \tag{3}$$

where V_f is the volume ratio, A_f is the surface area ratio, and V is the flow speed.

Because the free surface moves over time, the F value of each mesh grid must also change to reflect the surface position variations. We used a type of Donor-acceptor flux approximation to define the configurations of free surface. The key idea is to use information about F downstream as well as upstream of a flux boundary to establish an approximate interface shape and then to use this shape in computing the flux. A lot of free fluid surface motion calculations provided by the currently available CFD technique were developed using this method. The proposed numerical scheme is more comprehensive for free fluid surface modeling, which is known as the true VOF method. This allows mesh grids to be constructed easily, reduces memory usage, saves computer calculation time, and enables mesh grid elements to effectively adapt to common geometrical shapes.

2.3 FINITE DIFFERENCE SCHEME

This numerical method adopts the control volume-based finite difference method. Pressure is placed on the center point in the control volume, and velocity is placed on the surface of the control volume. The velocity terms are arranged in a staggered manner to conserve mass and accelerate the convergence rate during calculations. The solution of the time dependant Momentum equation (2) necessarily demands the use of an iterative solver. A generic form for the finite difference approximation of Equation (2) is written as

$$u_{i,j,k}^{n+1} = u_{i,j,k}^{n} + \Delta t^{n+1}[-\frac{p_{i+1,j,k}^{n+1} - p_{i,j,k}^{n+1}}{(\rho\delta x)_{i+\frac{1}{2},j,k}^{n}} + \varphi_x] \tag{4}$$

$$v_{i,j,k}^{n+1} = v_{i,j,k}^{n} + \Delta t^{n+1}[-\frac{p_{i,j+1,k}^{n+1} - p_{i,j,k}^{n+1}}{(\rho\delta y)_{i,j+\frac{1}{2},k}^{n}} + \varphi_y] \tag{5}$$

$$w_{i,j,k}^{n+1} = w_{i,j,k}^{n} + \Delta t^{n+1}[-\frac{p_{i,j,k+1}^{n+1} - p_{i,j,k}^{n+1}}{(\rho\delta z)_{i,j,k+\frac{1}{2}}^{n}} + \varphi_z] \tag{6}$$

where

$$(\rho\delta x)_{i+\frac{1}{2},j,k}^{n} = \frac{(\rho_{i,j,k}^{n}\delta x_i + \rho_{i+1,j,k}^{n}\delta x_{i+1})}{2}$$

$$(\rho\delta y)_{i,j+\frac{1}{2},k}^{n} = \frac{(\rho_{i,j,k}^{n}\delta y_j + \rho_{i,j+1,k}^{n}\delta y_{j+1})}{2}$$

$$(\rho\delta z)_{i,j,k+\frac{1}{2}}^{n} = \frac{(\rho_{i,j,k}^{n}\delta z_k + \rho_{i,j,k+1}^{n}\delta z_{k+1})}{2}$$

and φ_x, φ_y, φ_z include gravitational, rotational, general non-inertial acceleration, advective flux and viscous acceleration in the x,y,z-directions, respectively.

The solution of the pressure field demands the use of a guess-and-correct procedure on the staggered grid arrangement. The solution procedure can be simplified by making the discretized continuity equation as an equation for pressure correction δp . The pressure correction algorithm can be expressed as two steps

Velocity modification:

$$(u_{i+\frac{1}{2},j,k}^{n+1})^{N+1} = (u_{i+\frac{1}{2},j,k}^{n+1})^{N} + \Delta t\frac{(\delta p_{i,j,k}^{n+1})^N}{(\delta x_i + \delta x_{i+1})/2} \tag{7a}$$

$$(u_{i-\frac{1}{2},j,k}^{n+1})^{N+1} = (u_{i-\frac{1}{2},j,k}^{n+1})^{N} + \Delta t\frac{(\delta p_{i,j,k}^{n+1})^N}{(\delta x_i + \delta x_{i-1})/2} \tag{7b}$$

$$(v_{i,j+\frac{1}{2},k}^{n+1})^{N+1} = (v_{i,j+\frac{1}{2},k}^{n+1})^{N} + \Delta t\frac{(\delta p_{i,j,k}^{n+1})^N}{(\delta y_j + \delta y_{j+1})/2} \tag{8a}$$

$$(v_{i,j-\frac{1}{2},k}^{n+1})^{N+1} = (v_{i,j-\frac{1}{2},k}^{n+1})^{N} + \Delta t\frac{(\delta p_{i,j,k}^{n+1})^N}{(\delta y_j + \delta y_{j-1})/2} \tag{8b}$$

$$(w_{i,j,k+\frac{1}{2}}^{n+1})^{N+1} = (w_{i,j,k+\frac{1}{2}}^{n+1})^{N} + \Delta t\frac{(\delta p_{i,j,k}^{n+1})^N}{(\delta z_k + \delta z_{k+1})/2} \tag{9a}$$

$$(w_{i,j,k-\frac{1}{2}}^{n+1})^{N+1} = (w_{i,j,k-\frac{1}{2}}^{n+1})^{N} + \Delta t\frac{(\delta p_{i,j,k}^{n+1})^N}{(\delta z_k + \delta z_{k-1})/2} \tag{9b}$$

N denotes the number of iterative index.
Pressure correction

$$(\delta p_{i,j,k}^{n+1})^N = -\mathrm{Div} \tag{10}$$

where

$$\mathrm{Div} = \frac{\partial}{\partial x}(uA_x) + \frac{\partial}{\partial y}(vA_y) + \frac{\partial}{\partial z}(wA_z) - \frac{R_s}{\rho}$$

With this modification, the numerical convergence conditions are satisfied by using the velocity modification (Eqs. 7-9) and Pressure correction (Eq. 10) in the discretized form as expressed by equations (7-9). Using the result from Eq. (10), the new estimate for the cell pressure is written as

$$p_{i,j,k}^{n+1} = p_{i,j,k}^{n+1} + \delta p_{i,j,k}^{n+1} \tag{11}$$

In order to ensure accuracy in the prediction of velocities and pressure, a MAC staggered grid system is used in the present numerical scheme. Since the velocities u, v and w are already known the resulting set of equations from equations (4-6) can be solved using the control volume finite difference method. The main advantage of the present numerical solution procedure is that it assures a divergence-free solution for the velocity field, in addition to achieving a second-order numerical accuracy and a significant reduction in the computational time.

2.4 WAVE-GENERATING BOUNDARY

The numerical model can propagate the determined incoming waves at the upstream boundary toward the downstream. The wave-generating boundary ensures that the wave is generated on the left side, which subsequently passes through the boundary toward the right. The current wave generation is based on the linear wave theory. The given parameters include the wave amplitude A and the period time T.

Table 1 KCS geometric data of the actual vessel and ship model

Parameter item	Actual
Scale ratio λ	1
Length between perpendiculars L_{PP}(m)	230
Breadth B(m)	32.2
Draft T(m)	10.8
Displacement Δ(tons)	53330
Displacement volume ∇ (m^3)	52030
Wetted surface area S(m^2)	9424
Block Coefficient C_B	0.651
Prismatic coefficient C_P	0.661
Metacentric height $\overline{GM}$ (m)	7.326
L_{PP}/B	7.143
B/T	2.981
g acceleration of gravity (m/s^2)	9.81
ρ fluid density (kg/m^3)	1025
Center of mass x(m)	111.6
Center of mass y(m)	0.0
Center of mass z(m)	5.9

2.5 DOMAIN USED FOR THE NUMERICAL COMPUTATION

The ship model used in this study was a 3600 TEU Panamax container ship. The KCS ship model data (KRISO 3600 TEU Container Ship) was established using the CAD technique. Geometric data of the actual vessel and the ship model are shown in Table 1. To eliminate the shallow water effect and the interference of boundary reflection waves, the width and depth settings of the numerical navigation path modeled in this study follows the recommendations of the International Towing Tank Conference (ITTC). The ratio between the depth and the draft of the ship model should be at least 4 for deep water ($h/T > 4$). The width should be at least 8 times the ship breadth (B). Because the angle of incidence for waves varies throughout the simulation, this study modelled three navigation paths, all with a 45-meter depth. The wave incidence angles θ were 0, 45, and 90 degrees. Figure 1 shows the diagram of numerical navigation path with a various wave incidence angle. The wave considered in this study is T=9 s (period). With h= 9 m and T=9 s, the wave length at present case is λ=123.6 m. The wave boundary condition is used at left-hand side, others refers to the Outflow boundary.

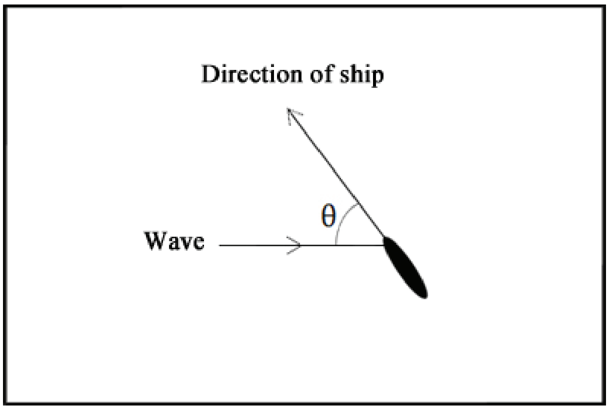

Figure 1 Diagram of numerical navigation path with a various wave incidence angle

Mesh blocks of the numerical navigation path were constructed using the Cartesian coordinate system, which defines the X direction as length, Y direction as width, and the Z direction as depth. Following the section on verifying the mesh block optimizations of the proposed model, and under computational power constraints of the available personal computers, this study restricted the mesh block numbers in the calculated region which yields approximately 10 million blocks.

3. METHODS

The ship model was created from the ship model geometric data and the offset table using CAD software. The numerical results were obtained by solving Navier-Stokes equations through a VOF Finite difference scheme. Decisions regarding the control parameters used in this modelling study are explained in the following section. Figure 2 shows the comparisons of vortical flow distribution in the midship cross-sectional plane of the ship model. The below figure of present study is agreement with the above figure in the literature [16].

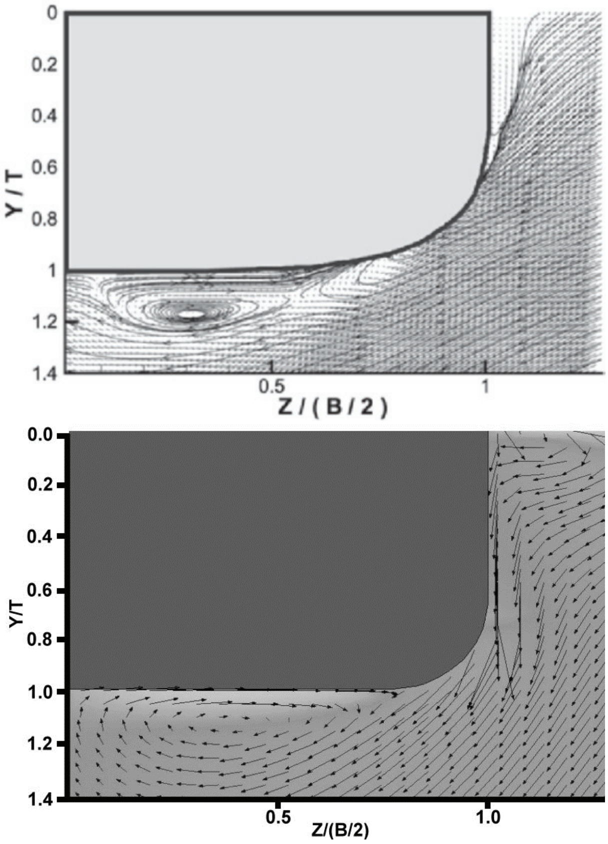

Figure 2 Vortical flow distribution in the midship cross-sectional plane of the ship model (The above figure is cited from a reference [16], whereas the below figure is the present simulation)

3.1 DETERMINING THE TEST SPEED FOR THE SHIP MODEL

In actual ship operations, when the vessels approach arrival pilot stations or anchorage areas, the vessels must employ the load-down program to decelerate from the sea or navigation speed to the maneuvering speed, loosing speed from the friction between the fluid and the ship model, the wave resistance, and the added mass. According to the model predictions in this study, when passing through fluid with the physical properties defined in our developed code (a single incompressible non-Newtonian fluid, with the water temperature at 20℃, density at 1025 kg/m^3, viscosity at 0.001 kg/m/s, gravity acceleration at -9.81 m/s^2, and atmospheric pressure at 1.013×10^5 Pa), the speed of the ship model is reduced by 30%.

3.2 DETERMINING SHIP MODEL TEST WAVE HEIGHT AND TEST WAVE HEIGHT AND CYCLE TIME

High sea waves are considered a random phenomenon that can be statistically characterized by probabilistic methods, or represented by wave spectrums. However, the complex growth process of waves is beyond the scope of this study. This study only considers single linear waves, ignoring oversized waves that exceed the height of the ship model to avoid the modelling inaccuracies that can result. Thus, the wave height in the modelling plan was set to under 5 m, with a period time of 9 s. The wave speed and wave length of a numerical navigation path with a 45-meter depth were 13.77m/s and 123.61 m.

3.3 DETERMINING THE WAVE INCIDENCE ANGLE FOR THE SHIP MODEL TEST

Vessels under wave disturbance at sea move in six degrees of freedom, which comprise the three linear motions heaving, surging, and swaying and the three rotational motions of rolling, pitching, and yawing around the three axes. Among these, heaving, rolling, and pitching are affected by restoring forces and restoring torques; thus, they are oscillatory motions. Surging, swaying, and yawing, however, are not affected by restoring forces or restoring torques; thus, they are non-oscillatory motions. To enable easy comparisons with literature on actual ocean navigation practices and the results from studies on transverse waves and oblique waves, and considering the loss of the ship model speed from various wave incidence angles, the incidence angles for the model are set at 0, 45, and 90 degrees.

4. RESULTS AND DISCUSSION

To verify that the number of grids was sufficient to model every case, we first divided the modeled case into further cells to verify the independence of the mesh blocks by determining whether similar model cases under different mesh blocks provide converging results. We compared the results using different mesh block numbers to model the same case and verified that the results are extremely similar. A comparison between the ship model's angular velocity and drag force is shown in Figure 3. In all the figures presented in this manuscript, D denotes the angle of wave incidence, and H denotes the wave height.

4.1 NUMERICAL INVESTIGATION WITH A 0-DEGREE WAVE INCIDENCE ANGLE AND WAVE HEIGHTS OF 0, 1, 3, AND 5 m

According to the numerical simulation results, this section presents the rolling, pitching, and yawing angular velocity changes under a 0-degree wave incidence angle and wave heights of 0, 1, 3, and 5 m when navigating the ship model. The change of the pitching angular velocity around the y axis of the ship model against the y axis of the center of mass was negative when rotating clockwise and positive when rotating counterclockwise. In Figure 4, because the ship instantly accelerated from a speed of zero to 10.3m/s, and under the frictional drag force of the fluid, the maximum value 0.016 rad/s at the initial navigation time. When the navigation time was 45 s, under the influence of the waves, the amplitudes of the ship model pitching up and down were approximately equal and did not change significantly with varying wave heights. However, the angle increases with increasing wave heights. The pitching cycle time does not decrease with increased wave height.

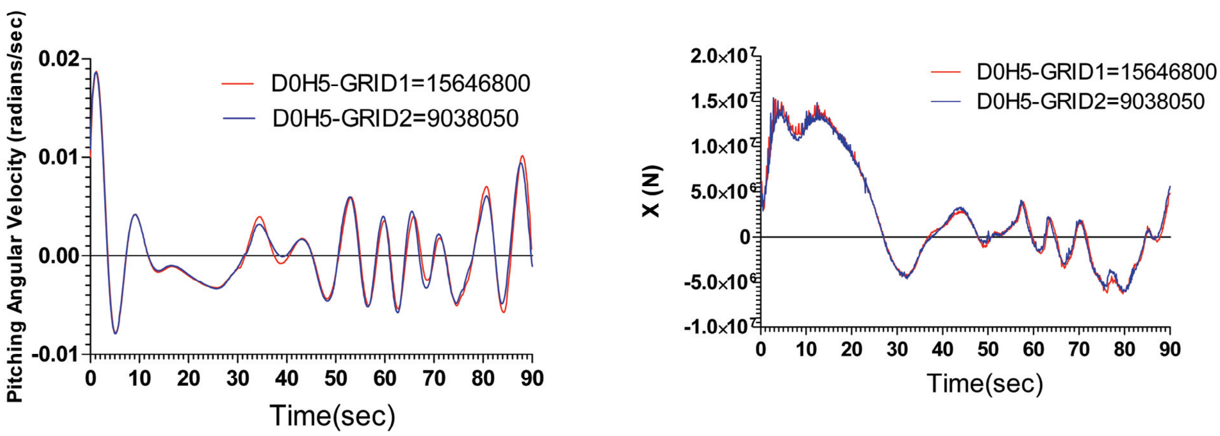

(a) (b)

Figure 3 Grid independence test (a) the rotational angular speed of ship models around the y axis, (b) drag force

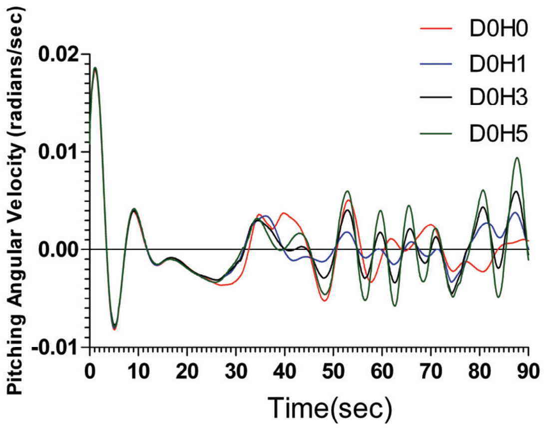

Figure 4 Under a wave incidence angle of 0 degrees, the change in hull rotations around the y axis (angular velocity)

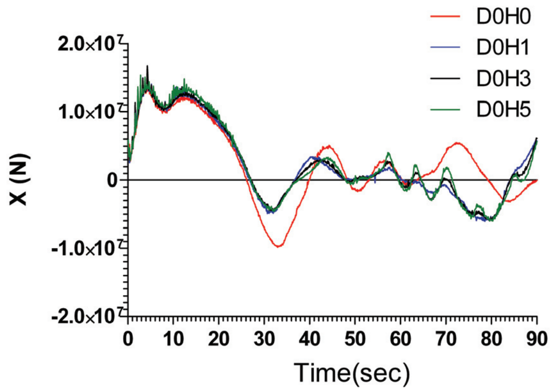

Figure 5 Under a wave incidence angle of 0 degrees, the changes in ship model drag force

Figure 5 shows that the value is positive when the ship model moves from the wave trough to the wave peak with increasing drag forces. However, the value is negative when the ship model moves from the wave peak to the wave trough with decreasing drag forces. When the ship model begins to advance at 10.3m/s in still water, the drag forces increase substantially during the first 3 s because of the fluid friction. The drag force encountered is greater when the wave height is higher. Figure 6 shows the navigation movements of the 3D ship model. The wave incidence angle was 0 degrees with a wave height of 5 m.

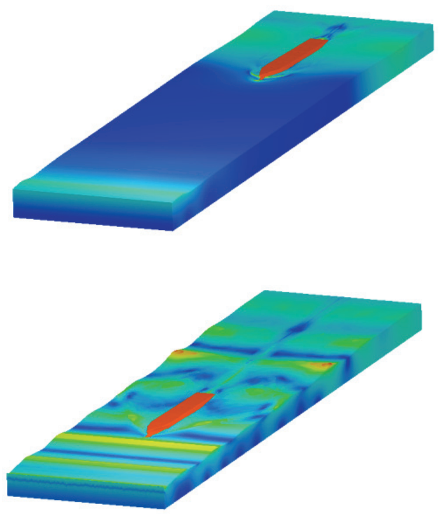

Figure 6 The ship model navigating movement demonstrations, with a wave incidence angle of 0 degrees and a wave height of 5 m

5.2 NUMERICAL INVESTIGATION WITH A 45-DEGREE WAVE INCIDENCE ANGLE AND WAVE HEIGHTS OF 0, 1, 3, AND 5 m

According to the numerical modeling results, we present the rolling, pitching, and yawing angular velocity changes under a 45-degree wave incidence angle and wave heights of 0, 1, 3, and 5 m when navigating the ship model. Changes in speed, drag force and swaying force are discussed in the final sections. In Figures 7(a) and 7(b), the rolling amplitude changed significantly with varying wave heights. Because the port side of the model received the incoming wave, the right rolling amplitudes were larger than the left rolling amplitudes. The maximum angle occurred at a wave height of 5 m and a navigation time of 58 s. The rolling cycle time decreases with increasing wave height.

In Figures 8(a) and 8(b), because the ship body instantly accelerated from a speed of zero to 10.3m/s, and under the frictional drag force of the fluid, the maximum angular velocity value 0.01 (1.9 degrees) occurred at the beginning. When the navigation time was 30 s, the angular velocity increased with increasing wave height. The maximum value occurred at a wave height of 5 m and a navigation time of 43 s. Under different wave heights, the amplitude of the ship model pitching up and down was approximately equal and did not change significantly with different wave heights. The average angle of the ship model pitching upward was larger than the average downward pitching angle. The maximum angle occurred when the navigation time was 40 s and at 2 degrees pitch up. The pitching cycle time increased with greater wave heights.

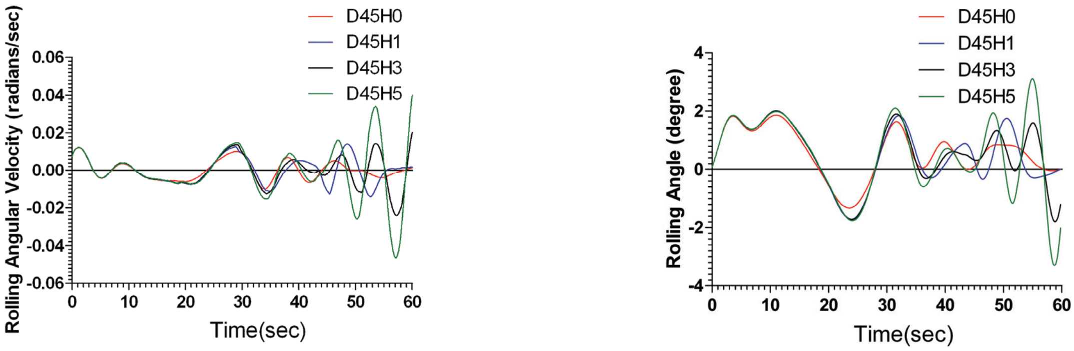

(a) (b)

Figure 7 Under a wave incidence angle of 45 degrees, the change in hull rotations around the x axis (a) angular velocity and (b) rolling angle

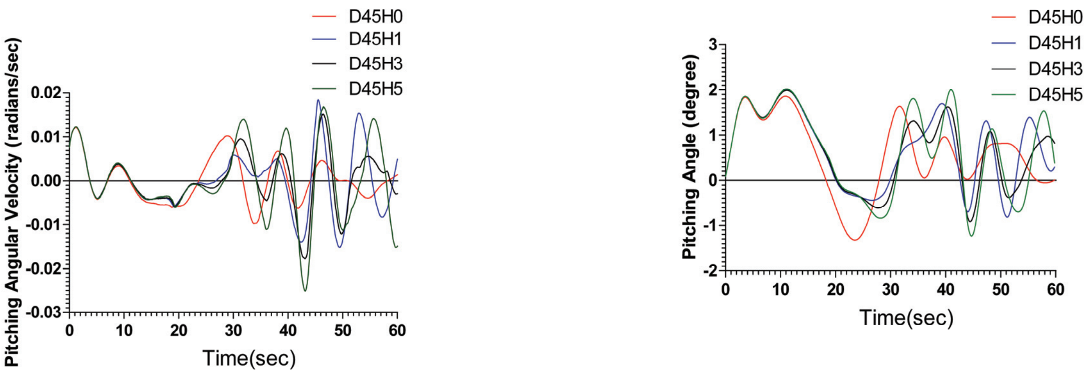

(a) (b)

Figure 8 Under a wave incidence angle of 45 degrees, the change in hull rotations around the y axis (a) angular velocity and (b) pitching angle

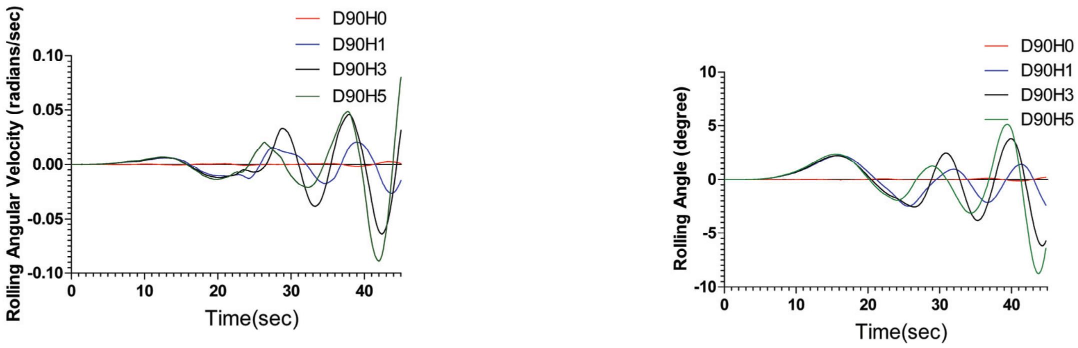

(a) (b)

Figure 9 Under a wave incidence angle of 90 degrees, the change in hull rotations around the x axis (a) angular velocity and (b) rolling angle

5.3 NUMERICAL INVESTIGATION WITH A 90-DEGREE WAVE INCIDENCE ANGLE AND WAVE HEIGHTS OF 0, 1, 3, AND 5 m

According to the numerical simulation results, this study presents the rolling, pitching, and yawing angular velocity changes under a 90-degree wave incidence angle and wave heights of 0, 1, 3, and 5 m when navigating the ship model. Changes in speed, drag force and swaying force are discussed in the final sections. In Figures 9(a) and 9(b), the rolling amplitude changed significantly with varying wave heights. Because the port side of the model received the incoming wave, the right rolling amplitudes were larger than the left rolling amplitudes.

The maximum angle occurred at a wave height of 5 m and a navigation time of 42 s. The rolling cycle time decreased with greater wave height.

6. CONCLUSIONS

This study modeled the interaction between a vessel and waves during navigation. The results indicate the following:

1. When sailing upward against waves with an incidence angle of 0 degree, the ship speed decreased significantly with increasing wave heights. However, at wave incidence angles of 45 and 90 degrees, increasing wave height had minimal influence on the ship speed lost.
2. Increasing wave height increases the drag force. However, when the wave incidence angles increased, the drag force decreased. This means that at the same wave height of 5 m, the drag force when the incidence angle is 0 is larger than when the drag force is 45 degrees, which is similarly larger than the drag force at 90 degrees.
3. Under various wave incidence angles, the increase in wave height increases the deflection of the navigation course. At the same wave height, larger wave incidence angles generate larger course deviations. At a wave incidence angle of 45 degrees, the course shifted to the right, with the bow turning toward the right, because the portside received the waves. At a wave incidence angle of 90 degrees, the course deviated to the right and the bow turned toward the left.
4. Considering the overall modeling result of this study, vessels advancing obliquely in waves should avoid advancing at a 90-degree angle to the wave propagation direction. This reduces the rolling and heaving, which can reduce ship stability and affect navigation safety.
5. When advancing in oblique waves, without considering the effects of the wind and currents, if the ship must turn as an avoidance maneuver, because of the constrained water area, large-angle turns away from the incoming wave direction should be considered. This is because when advancing obliquely in waves, ships have already employed the rudder against the side with the incoming wave to maintain their course. Thus, using the rudder to turn away from the wave should be considered because turning with a smaller turning circle is easier.
6. When advancing in transverse waves, meaning the course direction is perpendicular to the wave direction, if the ship must turn or avoid the wave in constricted water, turning into the direction of the wave with large-angle turns should be considered. This is because when advancing with transverse waves, ships have already employed the rudder to turn away from the incoming waves. Thus, when aiming to turn, the ship should turn in the direction of the incoming wave, which increases the ease of turning using a smaller turning circle.
7. When ships are advancing against the waves, if the wave height is excessive, the course direction should be changed. This is to avoid losing speed from severe pitching and reduce the substantial stress exerted on the hull, which may affect ship safety.

7. ACKNOWLEDGEMENTS

The support by the National Science Council, Taiwan under the grant no. NSC 100-2221-E-022-015 for the work is gratefully acknowledged.

8. REFERENCES

1. HOOYER, H.H. Behavior and Handling of Ships, *Cornell Maritime Pr/Tidewater Pub*, 1983.
2. LO, D.C., SU, D.T., CHEN, J. M. Application of computational fluid dynamics simulations to the analysis of bank effects in restricted water, *J Navigation, Volume 62, pp 477-491*, 2009.
3. LO, D.C., Numerical simulation of hydrodynamic interaction produced during the overtaking and the head-on encounter process of two ships, *Eng Comput, Volume 29, pp 83-101*, 2012
4. LEWIS, E.V., Numerate, E., Ship Motions in Oblique Sea, *SNAME 68*, 1960.
5. OCHI, M.K., Extreme Behavior of a Ship in Rough Sea –Slamming and Shipping of Green Water, *SNAME 72*, 1964.
6. KORVIN-KROUKOVSKY, B.V., Theory of Seakeeping, *SNAME*, 1961.
7. TASAI, F., TAKAKI, M., Theory and Calculation of Ship Response in Regular Waves, *Sym on Deavorthiness of Ships, JSNA*, 1969.
8. SALVENSEN, N., TUCK, E.O., FALTINSEN, O., Ship Motions and Sea Loads, *SNAME*, 1970.
9. WILSON, R.V., CARRICA, P.M., STEM, F., Simulation of ship breaking bow waves and induced vortices and scars, *Int J Numer Meth Fluids, Volume 54, pp 419–451*, 2007.
10. CAMPANA, E.F., PERI, D., TAHARA, Y., STERN, F., Shape optimization in ship hydrodynamics using computational fluid dynamics, *Comput Meth Apply Mech Eng, Volume 196, pp 634–651*, 2006.
11. ECA, L., HOEKSTRA, M., On the numerical accuracy of the prediction of resistance coefficients in ship stern flow calculations, *J Mar Sci Technol, Volume 14, pp 2–18*, 2009.

12. TOXOPEUS, S.L., Deriving mathematical manoeuvring models for bare ship hulls using viscous flow calculations, *J Mar Sci Technol, Volume 14, pp 30–38*, 2009.
13. DELEFORTRIE, G., VANTORRE, M., Prediction of the forces acting on container carriers in muddy navigation areas using a fluidization parameter, *J Mar Sci Technol, Volume 14, pp 51–68*, 2009.
14. GUO, B.J., STEEN, S., DENG, G.B., Seakeeping prediction of KVLCC2 in head waves with RANS, *Applied Ocean Res, Volume 35, pp 56-67*, 2012.
15. HIRT, C.W., NICHOLS, B.D., Volume of fluid (VOF) method for free boundaries, *J Comput Phys, Volume 39, pp 201-225*, 1981.
16. LEE, S.J., KOH, M.S., LEE, C.M., PIV velocity field measurements of flow around a KRISO 3600TEU container ship model, *J Mar Sci Technol, Volume 8, pp 76–87*, 2003.